Pulsed Laser Deposition of two-dimensional ZnO nanocrystals on Au(111): Growth, surface structure and electronic properties

F Tumino, C S Casari, M Passoni, C E Bottani and A Li Bassi

Department of Energy, Politecnico di Milano, piazza Leonardo da Vinci 32, I-20133 Milano, Italy

E-mail: `francesco.tumino@polimi.it`

E-mail: `andrea.libassi@polimi.it`

Abstract. Two-dimensional (2D) ZnO structures have been deposited on the Au(111) surface by means of the pulsed laser deposition (PLD) technique. *In situ* scanning tunneling microscopy (STM) and spectroscopy (STS) measurements have been performed to characterize morphological, structural and electronic properties of 2D ZnO at the nanoscale. Starting from a sub-monolayer coverage, we investigated the growth of ZnO, identifying different atomic layers (up to the 5th). At low coverage, we observed single- and bi-layer nanocrystals, characterized by a surface moiré pattern that is associated to a graphene-like ZnO structure. By increasing the coverage, we revealed a morphological change starting from the 4th layer, which was attributed to a transition toward a bulk-like structure. Investigation of the electronic properties revealed the semiconducting character of 2D ZnO. We observed a dependence of the density of states (DOS) and, in particular, of the conduction band (CB) on the ZnO thickness, with a decreasing of the CB onset energy for increasing thickness. The CB DOS of 2D ZnO shows a step-like behaviour which may be interpreted as due to a 2D quantum confinement effect in ZnO atomic layers.

1. Introduction

Since the discovery of graphene and its unique properties [1], intense research has been devoted to the study and application of two-dimensional (2D) materials. Recent years have witnessed a remarkable expansion of the family of 2D materials beyond graphene, with the synthesis of novel single- and few-layers atomic crystals that exhibit peculiar electronic and optical properties [2]. In particular, 2D oxides have attracted interest as promising candidates for engineering functional nanofilms and heterostructures with a wide range of applications, such as in nano-electronics [3], catalysis [4], photocatalysis [5] and biosensing [6]. Increasing effort is being focused on the investigation of the fundamental physics of 2D oxides as well as on the development of novel synthesis strategies, with the aim to design scalable and controlled processes. For instance, chemical methods based on liquid-phase exfoliation or molecular self-assembly have

been recently studied, allowing the production of oxide nanosheets [7, 8, 9]. However, the most exploited approach for the study of 2D oxides still relies on direct growth on metallic substrates, *via* physical or chemical vapour deposition. Traditionally, highly crystalline oxide thin films supported by metal substrates have been used as model systems for surface science investigations of physical phenomena occurring at oxide surfaces and metal-oxide interfaces. It is now well established that, in such systems, low-dimensionality, quantum confinement and interaction with the substrate contribute to the emergence of morphological, structural and electronic properties, in general, very different from those of corresponding bulk oxide surfaces [10]. High spatial resolution techniques, such as scanning tunneling microscopy (STM), have allowed to investigate these properties at the nanoscale, providing several examples of the large variety of novel 2D structures that can be observed in low-dimensional metal-supported oxide systems (e.g. for titanium [11], vanadium [12], iron [13], copper [14]).

Among transition metal oxides, zinc oxide (ZnO) has been extensively studied due to its remarkable electronic and optical properties, such as high exciton binding energy (60 meV at room temperature) and direct band gap (3.37 eV at room temperature), which make this material of fundamental importance for optoelectronic applications [15]. The most stable form of bulk ZnO is the wurtzite structure. However, the stability of a novel graphene-like structure (g-ZnO), with Zn and O atoms arranged in planar honeycomb geometry, has been recently predicted [16]. From theoretical investigations, the stability of free-standing g-ZnO is limited to few atomic layers (three, according to ref. [18]) and can be increased under epitaxial tensile strain [17]. The band gap is larger than in wurtzite ZnO and decreases with increasing thickness [20]. Tusche et al. [21] provided experimental evidence for the formation of g-ZnO on Ag(111) by means of pulsed laser deposition (PLD). Although the synthesis of quasi-free-standing ZnO membranes has been recently reported [24], g-ZnO has been mainly observed on metal (111)-oriented surfaces (e.g. Pd(111) [22], Pt(111) [23], Au(111) [25, 26, 27, 28]). A common feature revealed by these experimental works is the typical hexagonal moiré pattern observed on the g-ZnO surface, arising from the periodic coincidence between the honeycomb ZnO lattice and the (111) substrate lattice. This pattern changes around the thickness of the 4th layer [27] while the band gap approaches the bulk value [26], suggesting a transition to the wurtzite structure. Although the attention toward 2D ZnO is constantly growing and preliminary results have been reported, the experimental work is still in its early stages. The electronic properties have not been extensively investigated and a more detailed study of the first stages of growth is needed to gain insight into the growth mechanisms as well as into the transition to the bulk-like structure.

In this work we investigate the growth of 2D ZnO on Au(111) deposited by means of the PLD technique. We characterized the morphological, structural and electronic properties by means of *in situ* STM and STS measurements. Although PLD is a well established deposition technique for the growth of both pure and doped ZnO thin films [29], it has been scarcely explored for the deposition of 2D nanofilms, in comparison to other physical vapor deposition (PVD) techniques, e.g. based on thermal or e-beam evaporation. However, PLD is a versatile technique which has proved to be effective for fundamental investigation of simple model systems [30] as well as for the development of scalable approaches for the synthesis of 2D materials, such as graphene [31], transition metal dichalcogenides [32, 33] and hexagonal boron nitride [34]. Our experiments explore the applicability of such approach in the investigation of the first

stages of growth of 2D ZnO, starting from a sub-monolayer coverage. Morphological and structural characteristics are discussed in section 3.1, while section 3.2 focuses on the electronic properties of ZnO layers, providing insight into the characteristics of the electronic density of states (DOS).

2. Experimental methods

All experiments have been carried out in a ultra-high vacuum system (base pressure 2×10^{-11} mbar) composed of three interconnected chambers for sample preparation, pulsed laser deposition and STM analysis. The (111) surface of epitaxially grown Au on mica (Phasis Sàrl) has been cleaned by Ar^+ sputtering (1 keV) and annealing (700 K), before ZnO deposition. STM measurements ensured the formation of a clean surface with wide terraces (>100 nm) and the characteristic *herringbone* reconstruction, originating from the regular alternation of fcc and hcp domains separated by discommensuration lines [35]. ZnO deposition has been performed in a dedicated PLD chamber using a stoichiometric ZnO target (Kurt J. Lester Company Ltd, 99.999% pure) and a KrF excimer laser emitting 20 ns pulses with a wavelength of 248 nm. During deposition the substrate has been kept at room temperature and placed at 5 cm from the target. We chose a repetition rate of 1 pulse per second in order to accurately control the total number of ablating pulses. Target ablation has been achieved with a 0.5 J/cm^2 laser fluence. In the initial part of the experimental campaign, several experiments have been performed in order to investigate the effect of the background O_2 pressure during ZnO deposition. In the range from 10^{-8} to 10^{-1} mbar we did not observe any significant difference on the sample morphology in the investigated coverage range (data not shown). However, since it is known that PLD of oxides under high vacuum may produce oxygen deficient films [36], we performed depositions in a background oxygen atmosphere of 5×10^{-3} mbar in order to minimize the risk of oxygen deficiency in the deposited structures. After deposition, the sample was transferred in the preparation chamber where a two-step thermal treatment was performed, using previously reported recipes [25] as reference for the proper annealing temperature. In details, samples have been annealed at 540 K for 20 minutes in O_2 atmosphere (5×10^{-6} mbar) and for additional 10 minutes at 570 K in UHV to favour the desorption of excess oxygen, thus allowing more stable STM measurements. Annealing at higher temperatures results in a significant loss of deposited ZnO, probably due to desorption from the substrate.

STM and STS measurements have been performed with an Omicron VT-SPM at room temperature, using a electrochemically etched tungsten tip. STM images have been acquired in constant-current mode and subsequently analysed using a software for STM data analysis (Gwyddion [37]). Bias voltage (referred to the sample) and current set-point are reported in the caption of every STM image shown hereinafter. Differential conductivity (dI/dV) has been measured using a lock-in amplifier applying a modulation voltage of 43 mV$_{rms}$ at 6 kHz. $I(V)$ and $dI/dV(V)$ curves have been acquired simultaneously in open feedback-loop condition. Several spectra (at least 20) have been acquired for each investigated point and then averaged in order to increase the signal-to-noise ratio. We avoided taking STS spectra at positions too close to the border regions of ZnO crystallites, which may be characterized by a different local electronic structure due to edge states. When specified in the text, dI/dV curves have been normalized over a proper exponential tunneling coefficient, following a method originally proposed by Ukraintsev [38] and further elaborated by some of us [39].

Normalization aims to remove from STS spectra the exponential tail of the tunneling coefficient which often masks the electronic DOS.

3. Results and discussion

The growth of ZnO nanostructures was investigated by increasing, from 1 to 20, the number of ablating laser pulses. In the following section we will describe the evolution of the system and the morphological and structural properties as revealed by STM images. Section 3.2 is focused on the electronic characteristics as revealed by differential conductivity STS measurements.

### 3.1. Growth, morphology and structural properties

The effect of the annealing treatment is shown in figure 1, in which we compare STM images of the sample obtained after 1 laser pulse before and after annealing. In the as-deposited sample (figure 1(a)), we observe amorphous islands uniformly distributed on the substrate, with a preference for nucleation on the Au(111) regions with fcc stacking (inset). Most of these islands are composed of a base layer, ~ 2 Å thick, and small second-layer clusters growing on top of it, which are ~ 3.7 Å high with respect to the substrate. The average lateral dimension of the islands deposited on the gold surface (figure 1(a)) is 3.3 nm. We analysed STM images to obtain the total projected area of each layer on the substrate surface, which represents the relative coverage expressed as equivalent mono-layers (ML), where 1 ML corresponds to the surface atoms density of Au(111)-(1×1) (i.e. 1.4×10^{15} cm^{-2}). In samples observed before annealing (figure 1(a)), first and second layer coverages are 0.16 ML and 0.03 ML respectively.
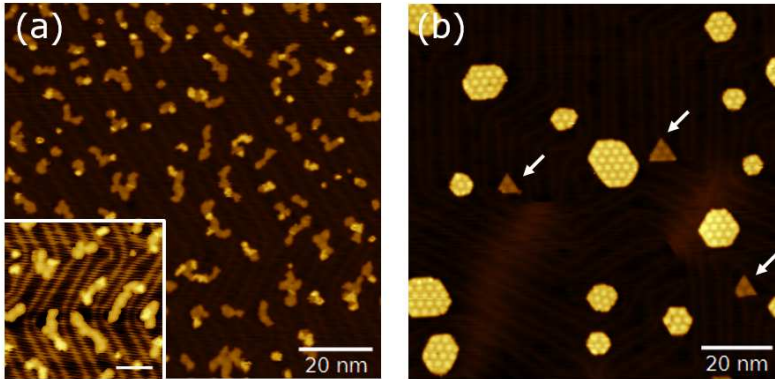
Figure 1. STM images ($V = 2.5$ V, $I = 1$ nA) of the sample obtained by hitting the ZnO target with 1 laser pulse. Images show the sample morphology before (a) and after (b) the post-deposition annealing. Inset of (a) is displayed in non-linear colour contrast to enhance the visibility of the substrate. ZnO islands preferentially nucleate on fcc regions of Au(111) (scale bar: 10 nm). White arrows in (b) indicate triangular-shaped single-layer nanocrystals.

After annealing, we observe the formation of well ordered nanocrystals (figure 1(b)): the majority of them have hexagonal shape, but there are also smaller

triangular crystallites (indicated by white arrows). The latter are $\sim$ 2 Å thick, while the former $\sim$ 3.7 Å, values very similar to first and second layer thickness before annealing. The surface of both kinds of crystallites is characterized by a hexagonal moiré pattern that can be considered as the fingerprint of graphene-like ZnO formation on (111) metal surfaces, as reported in other works [21, 22, 25]. Calculated values for the interlayer distance in graphene-like ZnO range between 2 and 2.4 Å [40, 19]. Accordingly, we associate triangular crystallites to single-layer ZnO, while the hexagonal ones to bi-layer ZnO, in agreement with recently reported experimental data [26]. In comparison to the sample observed before annealing, the coverage of the 1st layer decreases down to 0.09 ML while that of the 2nd layer increases up to 0.07 ML. Overall, the total coverage, i.e. the sum of 1st and 2nd layer coverages (0.16 ML), decreases, suggesting that a certain amount of deposited material is loss due to thermally induced desorption and/or bulk interdiffusion. Upon annealing, the 2nd layer coverage increases at the expense of the 1st, revealing a preference for 2D ZnO to form bi-layer structures rather than wetting the gold surface with a single-layer film. This growth mechanism is probably driven by the much higher ZnO interlayer interaction energy with respect to adhesion energy on Au(111), as predicted by theoretical calculations [25].
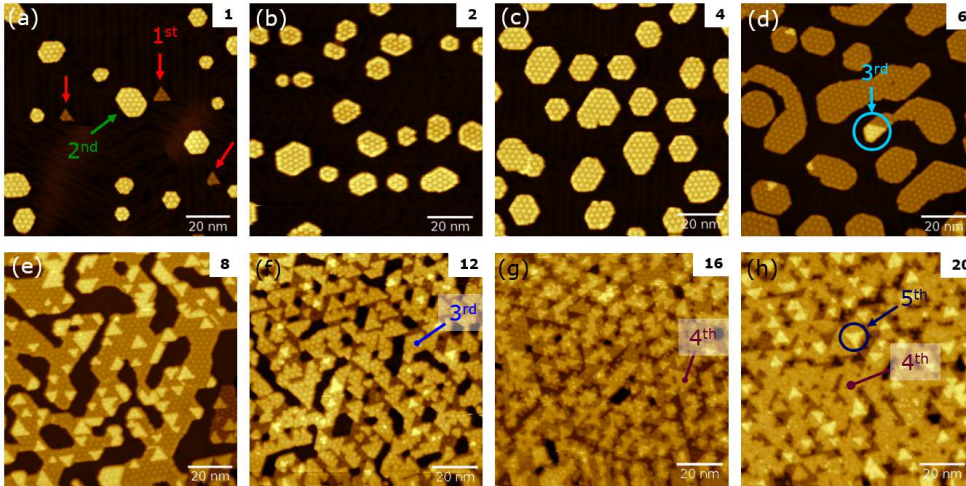

Figure 2. STM images at different coverage showing the growth of ZnO structures for increasing number of laser pulses. Samples were obtained for (a) 1, (b) 2, (c) 4, (d) 6, (e) 8, (f) 12, (g) 16 and (h) 20 laser pulses (as indicated at the top-right corner of each image). Frame size: 100×100 nm^2. Set-point parameters: $V = 2.5$ V, $I = 1$ nA. Labels indicate ZnO layers from the 1st to the 5th.

Large-scale STM images (100×100 nm^2) in figure 2 provide an overview of the growth of ZnO nanostructures as the number of laser pulses increases from 1 to 20 (the corresponding number is shown at the top-right corner of each image). Triangular-shaped single-layer islands are observed only for 1 pulse (figure 2(a)). For 2-4 pulses (figure 2(b)-(c)), we observe bi-layer islands, mostly hexagonal, which increase in size and then start to coalesce. The growth of third layer crystallites, with a thickness of $\sim$ 2 Å, measured with respect to the 2nd layer, is clearly revealed for 6 pulses

(figure 2(d)). Gradually, the bi-layer coalescence leads to the formation of an almost continuous film, on top of which the third layer expands (8 pulses, figure 2(e)). For increasing number of laser pulses (from 12 to 20), the ZnO film evolves with the growth of the 4th and 5th layers (figure 2(f)-(h)).

In figure 3 we plotted the partial coverage of ZnO layers *versus* the total coverage (figure 3) to quantitatively analyse the evolution of the system. We also reported the theoretically calculated coverages (dashed lines) of the first five layers obtained from a simple *birth-death* model that assumes the growth rate of the n-th layer proportional to the exposed surface of the (n-1)-th layer [41]. Although this model does not explicitly take into account important mechanisms and parameters (e.g. surface and interlayer diffusion), it may be tentatively applied to describe a film growth deviating from layer-by-layer mode. However, in our case, the significant disagreement between model and experimental data can be considered as evidence for the fundamental role that interaction with the substrate and interaction among different ZnO layers play in determining the evolution of the system. Indeed, apart from the lowest coverage region, where we revealed nanocrystals composed only by a single ZnO layer, the 1st and 2nd layer coverages are always coincident, due to the early formation of bi-layer structures. The behaviour of subsequent layers, whose coverage is initially lower and then becomes higher than the theoretical one, suggests that an interlayer diffusion mechanisms is at work, retarding the growth of a particular layer in favour of the lower.
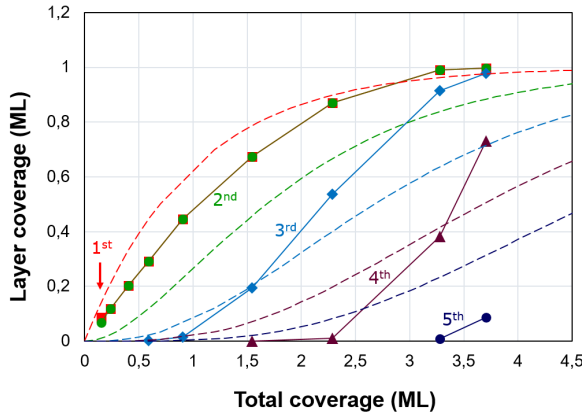
Figure 3. Layer coverage of each ZnO layer is plotted *versus* the total coverage. Dots represent experimental data. Dashed lines are theoretical coverages obtained from a *birth-death* growth model [41]. The layer number is reported near the corresponding coverage data. Each colour represents a specific layer according to the following legend: red: 1st layer; green: 2nd; blue: 3rd; purple: 4th; deep blue: 5th.

High-resolution STM images allow us to characterize in detail morphological and structural properties of the observed ZnO structures. Single- and bi-layer nanocrystals are shown in figure 4(a). In both structures the moiré superlattice is aligned with the Au(111) symmetry directions, i.e. $\langle 1\bar{1}0 \rangle$. The topographic profile in figure 4(b) highlights the height difference. Figure 4(c) shows an atomic resolution STM image of a single-layer nanocrystal. The hexagonal lattice is clearly resolved with a periodicity

of 3.4 ± 0.2 Å. The enhancement of edges is most probably due to a different local electronic structure associated to edge states. Figure 4(d) shows bi-layer crystallites. The one labelled by A exhibits the usually observed moiré pattern, having a periodicity of 22 ± 0.7 Å (figure 4(e), blue dashed line). Occasionally, we observed nanocrystals showing a different moiré pattern (e.g. the one labelled by B in figure 4(d)), characterized by a lower periodicity of ~ 13 Å (figure 4(e), red line) and different orientation. This superlattice may originate from a less stable configuration where the stacked lattices are misaligned, albeit theoretical modelling would be necessary in order to provide a more quantitative interpretation. Figure 4(f) shows an atomic resolution of a bi-layer nanocrystal with the usual moiré pattern. As highlighted in the image, the ZnO cell and the moiré supercell are aligned with each other. A ZnO-(7×7)/Au-(8×8) coincidence structure well agrees with experimental data, as proposed in other works [25, 27]. Different atomic defects are also revealed on the ZnO surface, probably inducing a local modification of the atomic arrangement and electronic structure. The origin of such defects is presently unclear.
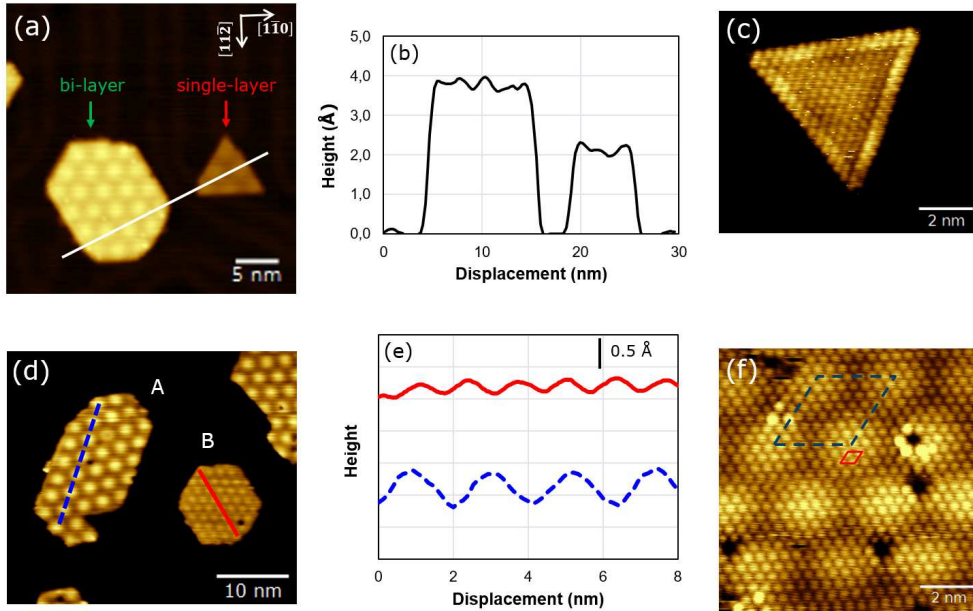
Figure 4. (a) STM image ($V = 2.5$ V, $I = 1$ nA) showing a triangular single-layer and a hexagonal bi-layer crystallite. (b) Height profile along the white line in (a). (c) Atomic resolution STM image of a single-layer crystallite ($V = 80$ mV, $I = 1.5$ nA). (d) STM image showing bi-layer crystallites ($V = 2.5$ V, $I = 1$ nA). Colour contrast has been enhanced to highlight the ZnO surface. Letters A and B indicate two crystallites characterized respectively by the usually observed moiré pattern and the unusual pattern with smaller periodicity and different orientation. (e) Height profiles along the corresponding lines in (d). Plots have been vertically separated for clarity. (f) Atomic resolution STM image of the surface of a bi-layer nanocrystal ($V = 0.5$ V, $I = 1$ nA) with the usual moiré periodicity. The blue dashed line indicates the moiré supercell, the red line the ZnO unit cell.

As the coverage increases (figure 5), the coalescence of bi-layer islands into an

almost continuous film is observed together with the growth of 3rd layer crystallites (figure 5(a)). Most of them are observed at the edges of the bi-layer film, suggesting that a different edge electronic structure results in locally higher interlayer interaction energy. The 3rd layer is also characterized by the same moiré pattern of the underlying layer. Figure 5(b) shows the growth of 4th layer islands, mostly triangular-shaped, having an apparent thickness of 2.3 Å. These islands do not exhibit the typical moiré that is clearly visible on the underlying layer. The surface morphology changes significantly for higher coverage (figure 5(c)), with the disappearing of the moiré pattern. The apparent thickness of the 4th layer increases to 3 Å and 5th layer triangular islands, with a thickness of 2.3 Å, start growing. This structural modification may represent the transition toward a bulk-like structure. In this respect, we note that the morphology is similar to the bulk ZnO(0001) Zn-terminated surface, characterized by triangular islands and pits arising from a particular depolarization mechanism [42].
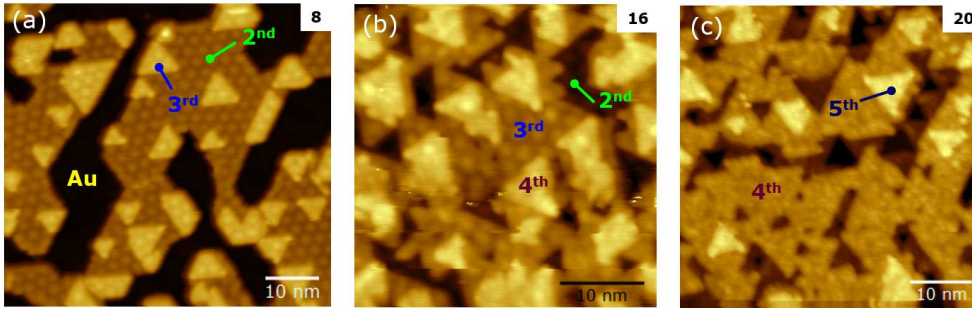
Figure 5. STM images of the samples obtained for (a) 8, (b) 12 and (c) 20 laser pulses (as reported at the top-right corner of each image). Measurements parameters: $V = 2.5\,\mathrm{V}$, $I = 1\,\mathrm{nA}$.

As a concluding remark of this section, we note that STM measures an *apparent* topography, which, in general, depends on the electronic properties of the investigated surface, in addition to the topographic corrugation. In this respect, we revealed an influence of the ZnO electronic properties on the measured layer thickness, as shown for instance for the 2nd layer in figure 6(a). The apparent height with respect to the substrate increases with bias voltage from 3.7 to 5.5 Å. Electronic effects have been also revealed in the corrugation of the moiré pattern. For instance, the moiré corrugation of the 2nd layer increases from 40 ± 5 pm at 1.5 V to 65 ± 5 pm at 2.5 V. Such dependence emerges clearly when comparing STM images taken with positive and negative bias voltages (figure 6(b)-(c)). As shown by figure 6(c), for negative voltage the moiré pattern disappears and the ZnO surface is almost perfectly planar. Since occupied sample states are imaged at negative bias, our measurements suggest that the moiré pattern is to be attributed mainly to a spatial modulation of the density of unoccupied electronic states rather than a topographic buckling.
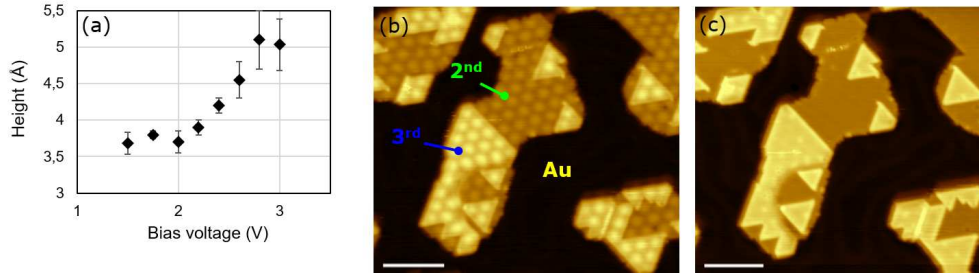
Figure 6. (a) Apparent height of the 2nd ZnO layer measured with respect to the substrate for varying bias voltage. (b)-(c) STM images of the same sample area taken with a bias voltage of 1 V and –1 V, respectively. Current set-point: $I = 1\,\mathrm{nA}$. Scale bar: 10 nm.

3.2. Electronic properties

Differential conductivity (dI/dV) maps and STS measurements provide useful information on the surface local electronic properties, in an energy range determined by the tip-sample voltage. In figure 7 we report STM images and simultaneous dI/dV maps of the same sample area, showing regions of bare Au, 2nd and 3rd ZnO layer (see labels in figure 7(a)). Interesting features are revealed by dI/dV
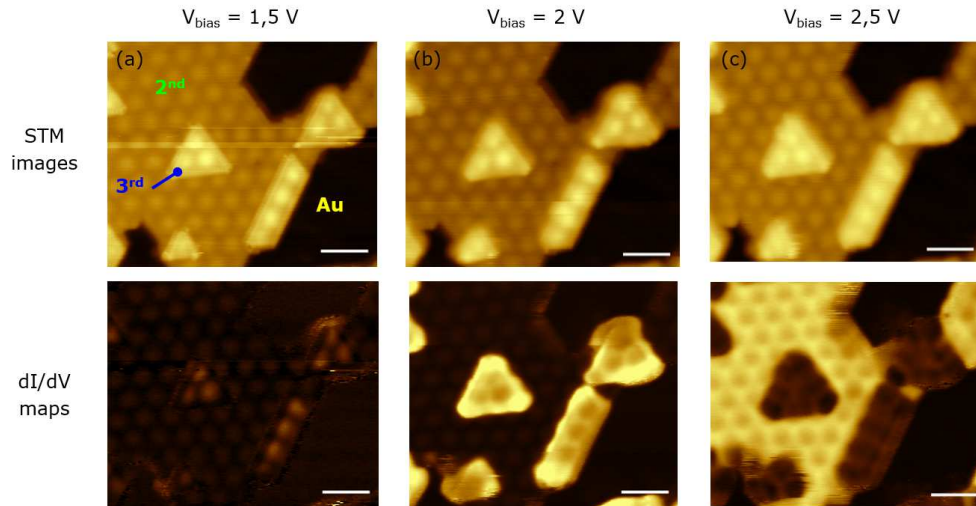

Figure 7. STM images (top) and corresponding dI/dV maps (bottom) taken at different bias voltage on the same sample area: (a) 1.5 V, (b) 2 V, (c) 2.5 V. Current set-point: $I = 1\,\mathrm{nA}$. Scale bar: 5 nm.

maps in the voltage range from 1.5 V to 2.5 V. At 1.5 V (figure 7(a), down) both ZnO layers show no significant contrast with respect to the substrate, excluding the moiré modulation, which is slightly enhanced in the 3rd layer. At 2 V (figure 7(b)) the differential conductivity of the 3rd layer significantly increases, while at 2.5 V (figure 7(c)) the major contribution to local conductivity originates from the 2nd layer. These data suggest the hypothesis that the onset of the conduction band of different ZnO layers occurs at different energy values, causing the observed increase

of tunneling conductivity and the consequent increase of apparent height. As it will be discussed below, STS data support this hypothesis and provide further insight into the electronic DOS. Interestingly, dI/dV maps show also that the increase in conductivity is accompanied by the inversion of the contrast of the moiré pattern, as further evidence for its electronic nature.

STS measurements have been performed on Au(111) and ZnO layers at different coverages in the investigated range. Since our measurements did not show significant variations with coverage, we averaged dI/dV curves in order to obtain, without loss of information, a single spectrum for each layer and the substrate, representative of its specific electronic DOS. The resulting STS spectra are shown in figure 8(a). The
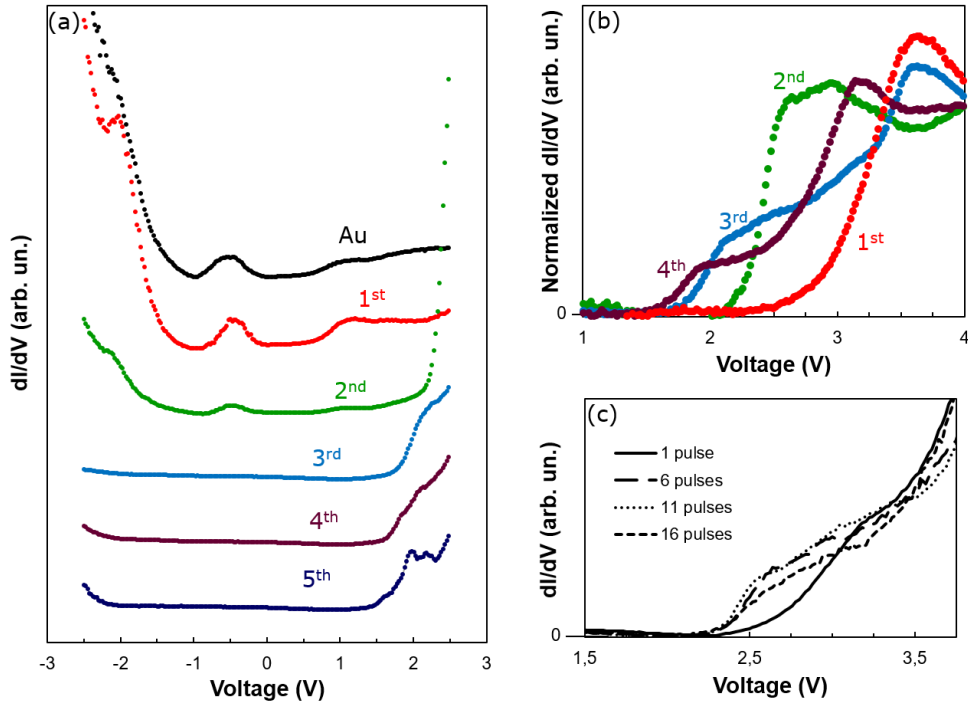
Figure 8. (a) dI/dV spectra of Au(111) and different ZnO layers, as indicated by corresponding labels. The curves have been vertically separated for clarity. Acquisition set-point: $V = 2.5\,\mathrm{V}$, $I = 1\,\mathrm{nA}$. (b) Normalized dI/dV spectra in the range from 1 to 4 V. Acquisition set-point: $V = 4\,\mathrm{V}$, $I = 1\,\mathrm{nA}$. (c) dI/dV spectra taken on the 2nd layer at different coverages. Acquisition set-point: $V = 4\,\mathrm{V}$, $I = 1\,\mathrm{nA}$.

Au(111) spectrum shows the characteristic Shockley state at about –0.5 V [43]. The dI/dV curve of the 1st layer is very close to that of Au(111), while in the 2nd the contribution of Au electronic states is weaker and a sharp increase in conductivity is revealed at 2.5 V, which can be attributed the onset of the ZnO conduction band (CB), in agreement with what observed in dI/dV maps (figure 7). The spectra of the 3rd, 4th and 5th layers show a typical semiconducting behaviour. The contribution of Au DOS, revealed in the 1st and, to a lesser extent, 2nd layer spectra, can be accounted for by the penetration of Au electronic wavefunctions across the gap region of ZnO. Since

we used always the same bias and current set-point to perform STS measurements, it seems reasonable to expect a progressive damping of Au electronic states due to the gradual increase of tip-Au distance as the thickness of ZnO increases. This may explain why the Au DOS is attenuated in the 2nd layer spectrum and no significant contribution is revealed in the spectra of the following layers. A closer look at the positive end of the voltage interval reveals that the onset of the ZnO conduction band occurs at increasingly lower voltages as the ZnO thickness increases. This result is in agreement with the reduction of the band gap for increasing number of layers which theoretical and experimental works have reported [20, 26]. A band gap of ~ 3.5 eV can be estimated from the 5th layer spectrum, compatible to the 3.37 eV bulk value.

To further investigate the energy range where the CB onset takes place, we performed STS measurements in the range from 1 to 4 V. The acquired dI/dV curves have been suitably normalized to better highlight the DOS features (see section 2). The resulting spectra (figure 8(b)) confirm the aforementioned dependence of the CB onset on ZnO thickness. In addition, they reveal particular features resembling "steps" of the electronic DOS. As shown by theoretical calculations [20], the step-like behaviour of the CB DOS can be due to 2D quantum confinement in ZnO layers. In principle, quantization effects can also arise from lateral confinement in small ZnO crystallites, as observed for instance in ZnO nanoclusters with zincblend structure [44]. The effect of lateral confinement is probably revealed only for small bi-layer nanocrystals at the lowest coverage, as suggested by STS spectra in figure 8(c). The average dI/dV curve of bi-layer islands observed for one laser pulse shows a shifted increase compared to the curves taken at higher coverages, i.e. when bi-layer structures coalesce into larger crystallites. However, apart from this observation, our STS measurements do not show a significant dependence on coverage, meaning that the electronic properties are not heavily affected by the lateral size of ZnO layers, in agreement with the hypothesis of a dominant 2D vertical confinement.

4. Conclusions

We studied the growth of 2D ZnO nanostructures on the Au(111) surface, synthesized by pulsed laser deposition. The morphological and structural properties were investigated by *in situ* STM for increasing coverage, allowing the identification of different ZnO atomic layers. At low coverage, we observed triangular single-layer and hexagonal bi-layer nanocrystals. Under our experimental conditions, the growth of bi-layer structures is favoured, leading to the formation, as coverage is increased, of a bi-layer film on top of which 3rd layer crystallites grow. Up to this point, the surface of ZnO layers shows a hexagonal moiré pattern with ~ 22 Å periodicity, which is associated to the formation of a graphene-like structure. The moiré pattern shows a significant bias dependence which suggests that it originates from a periodic spatial modulation of the density of unoccupied electronic states. Starting from the 4th ZnO layer, the moiré pattern is no longer visible, and a morphological change takes place, associated with the increase of the apparent thickness of the 4th layer. This transition may indicate the formation of the wurtzite ZnO(0001) surface with Zn termination, where different depolarization mechanisms occur.

The electronic properties of ZnO layers were investigated by means of STS measurements and dI/dV maps. A semiconducting behaviour is revealed, with a dependence of the conduction band onset on the ZnO thickness. In particular, as the layer thickness increases, the onset of the conduction band occurs at increasingly

lower energy. We also observed a step-like behaviour of the density of conduction band states that may be related to a 2D quantum confinement effect.

Our experiments provide insight into the synthesis of 2D ZnO by pulsed laser deposition and contribute to the study of the growth and the fundamental properties of this material.

Acknowledgments

References

[1] Novoselov K S, Geim A K, Morozov S V, Jiang D, Zhang Y, Dubonos S V, Grigorieva I V, Firsov A A 2004 *Science* **306** 666
[2] Butler S Z *et al.* 2013 *ACS Nano* **7** 2898–926
[3] Osada M and Sasaki T 2012 *Adv. Mater.* **24** 210–28
[4] Pacchioni G 2014 *Chem. Rec.* **14** 910–22
[5] Ida S and Ishihara T 2014 *J. Phys. Chem. Lett.* **5** 2533–42
[6] Shavanova K, Bakakina Y, Burkova I, Shtepliuk I, Viter R, Ubelis A, Beni V, Starodub N, Yakimova R and Khranovskyy V 2016 *Sensors* **16** 223
[7] Ma R and Sasaki T 2015 *Acc. Chem. Res.* **48** 136–43
[8] Sun Z, Liao T, Dou Y, Hwang S M, Park M, Jiang L, Kim J H and Dou S X 2014 *Nat. Commun.* **5** 3813
[9] Xiao X *et al.* 2016 *Nat. Commun.* **7** 11296
[10] Pacchioni G 2012 *Chem. Eur. J.* **18** 10144–58
[11] Tumino F, Carrozzo P, Mascaretti L, Casari C S, Passoni M, Tosoni S, Bottani C E and Li Bassi A 2015 *2D Mater.* **2** 045011
[12] Surnev S, Vitali L, Ramsey M G, Netzer F P, Kresse G and Hafner J 2000 *Phys. Rev.* B **61** 13945–54
[13] Yao Y, Fu Q, Wang Z, Tan D and Bao X 2010 *J. Phys. Chem.* C **114** 17069–79
[14] Sträter H, Fedderwitz H, Groß B and Nilius N 2015 *J. Phys. Chem.* C **119** 5975–81
[15] Özgür Ü 2005 *J. Appl. Phys.* **98** 041301
[16] Freeman C L, Claeyssens F and Allan N L 2006 *Phys. Rev. Lett.* **96** 066102
[17] Wu D, Lagally M G and Liu F 2011 *Phys. Rev. Lett.* **107** 236101
[18] Tu Z C and Hu X 2006 *Phys. Rev.* B **74** 035434
[19] Topsakal M, Cahangirov S, Bekaroglu E and Ciraci S 2009 *Phys. Rev.* B **80** 235119
[20] Kang J, Zhang Y, Wen Y H, Zheng J C and Zhua Z Z 2010 *Phys. Lett.* A **374** 1054–8
[21] Tusche C, Meyerheim H L and Kirschner J 2007 *Phys. Rev. Lett.* **99** 026102
[22] Weirum G, Barcaro G, Fortunelli A, Weber F, Schennach R, Surnev S and Netzer F P 2010 *J. Phys. Chem.* C **114** 15432–9
[23] Martynova Y, Liu B H, McBriarty M E, Groot I M N, Bedzyk M J, Shaikhutdinov S and Freund H J 2013 *J. Catal.* **301** 227–32
[24] Quang H T, Bachmatiuk A, Dianat A, Ortmann F, Zhao J, Warner J H, Eckert J, Cunniberti G and Mark H. Rümmeli M H 2015 *ACS Nano* **9**(11) 11408–13
[25] Deng X, Yao K, Sun K, Li W X, Lee J and Matranga M 2013 *J. Phys. Chem.* C **117** 11211–8
[26] Lee J, Sorescu D C and Deng X 2016 *J. Phys. Chem. Lett.* **7** 1335–40
[27] Stavale F, Pascua L, Nilius N and Freund H J 2013 *J. Phys. Chem.* C **117** 10552–7
[28] Zeng Y J, Schouteden K, Amini M N, Ruan S C, Lu Y F, Ye Z Z, Partoens B, Lamoen D and Van Haesendonck C 2015 *ACS Appl. Mater. Interfaces* **7** 10617–22
[29] Gondoni P, Ghidelli M, Di Fonzo F, Carminati M, Russo V, Li Bassi A and Casari C S 2012 *Nanotechnology* **23** 365706
[30] Casari C S, Foglio S, Passoni M, Siviero F, Bottani C E and Li Bassi A 2011 *Phys. Rev.* B **84** 155441
[31] Hemani G K, Vandenberghe W G, Brennan B, Chabal Y J, Walker A V, Wallace R M, Quevedo-Lopez M and Fischetti M V 2013 *Appl. Phys. Lett.* **103** 134102
[32] Siegel G, Venkata Subbaiah Y P, Prestgard M C and Tiwari A 2015 *APL Mat.* **3** 056103
[33] Loh T A J, Chua D H C and Wee A T S 2015 *Sci. Rep.* **5** 18116

[34] Glavin N R, Jespersen M L, Check M H, Hu J, Hilton A M, Fisher T S, Voevodin A A 2014 *Thin Solid Films* **572** 245–50
[35] Barth J V, Brune H, Ertl G, Behm R J 1990 *Phys. Rev.* B **42**(15) 9307–18
[36] Choopun S, Vispute R D, Noch W, Balsamo A, Sharma R P and Venkatesan T 1999 *Appl. Phys. Lett.* **75**(25) 3947–9
[37] Nečas D and Klapetek P 2012 *Open Phys.* **10**(1) 181–8
[38] Ukraintsev V A 1996 *Phys. Rev.* B **53** 11176–85
[39] Passoni M, Donati F, Li Bassi A, Casari C S and Bottani C E 2009 *Phys. Rev.* B **79** 045404
[40] Claeyssens F, Freeman C L, Allan N L, Sun Y, Ashfold M N R and Harding J H 2005 *J. Mater. Chem.* **15** 139–48
[41] Cohen P J, Petrich G S, Pukite P R and Whaley G J 1989 *Surf. Sci.* **216** 222–48
[42] Dulub O, Diebold U and Kresse G 2003 *Phys. Rev. Lett.* **90**(1) 016102
[43] Davis L C, Everson M P and Jaklevic R C 1991 *Phys. Rev.* B **43**(5) 3821–30
[44] Schouteden K, Zeng Y J, Lauwaet K, Romero C P, Goris B, Bals S, Van Tendeloo G, Lievens P and Van Haesendonck C 2013 *Nanoscale* **5** 3757–63